



# Cell type-specific attenuation of brassinosteroid signaling precedes stomatal asymmetric cell division

Eun-Ji Kim<sup>a,b,1</sup>, Cheng Zhang<sup>a,b,1,2</sup>, Boyu Guo<sup>a,b,c,1</sup>, Thomas Eekhout<sup>a,b,d,1</sup> , Anaxi Houbaert<sup>a,b,3</sup>, Jos R. Wendrich<sup>a,b</sup>, Niels Vandamme<sup>d</sup>, Manish Tiwari<sup>a,b,4</sup>, Claire Simon-Vezo<sup>a,b</sup>, Isabelle Vanhoutte<sup>a,b</sup>, Yvan Saeys<sup>e,f</sup>, Kun Wang<sup>a,b,c</sup>, Yuxian Zhu<sup>c</sup>, Bert De Rybel<sup>a,b,5</sup> , and Eugenia Russinova<sup>a,b,5</sup>

This contribution is part of the special series of Inaugural Articles by members of the National Academy of Sciences elected in 2022.

Contributed by Eugenia Russinova; received March 21, 2023; accepted July 16, 2023; reviewed by Ana Caño-Delgado, Stuart A. Casson, and Idan Efroni

In *Arabidopsis thaliana*, brassinosteroid (BR) signaling and stomatal development are connected through the SHAGGY/GSK3-like kinase BR INSENSITIVE2 (BIN2). BIN2 is a key negative regulator of BR signaling but it plays a dual role in stomatal development. BIN2 promotes or restricts stomatal asymmetric cell division (ACD) depending on its subcellular localization, which is regulated by the stomatal lineage-specific scaffold protein POLAR. BRs inactivate BIN2, but how they govern stomatal development remains unclear. Mapping the single-cell transcriptome of stomatal lineages after triggering BR signaling with either exogenous BRs or the specific BIN2 inhibitor, bikinin, revealed that the two modes of BR signaling activation generate spatiotemporally distinct transcriptional responses. We established that BIN2 is always sensitive to the inhibitor but, when in a complex with POLAR and its closest homolog POLAR-LIKE1, it becomes protected from BR-mediated inactivation. Subsequently, BR signaling in ACD precursors is attenuated, while it remains active in epidermal cells devoid of scaffolds and undergoing differentiation. Our study demonstrates how scaffold proteins contribute to cellular signal specificity of hormonal responses in plants.

brassinosteroids | *Arabidopsis* | stomatal development | single-cell RNA sequencing | asymmetric cell division

The steroidal phytohormones, brassinosteroids (BRs), are essential regulators of growth and development and their signaling pathway is one of the best-defined in plants (1). The *Arabidopsis thaliana* SHAGGY/GSK3-like kinase21 (*AtSK21*)/BR-INSENSITIVE2 (BIN2) is a key negative regulator of BR signaling because it inactivates two master transcription factors, BRASSINAZOLE RESISTANT1 (BZR1) and BRI1-EMS-SUPPRESSOR1 (BES1)/BZR2 via phosphorylation (2, 3). BR binding to the plasma membrane (PM)-localized BR receptor complex initiates a signaling cascade that leads to BIN2 inactivation and degradation through dephosphorylation by the phosphatase BRI1 SUPPRESSOR1 (BSU1) and ubiquitination by the F-box protein KINK SUPPRESSED IN BZR1-1D (KIB1), respectively (4, 5). Consequently, dephosphorylated BZR1 and BES1 translocate to the nucleus and regulate expression of target genes (6, 7).

BIN2 is also an important regulator of the stomatal development (8–11). In *Arabidopsis*, the stomatal lineage is initiated from an undifferentiated meristemoid mother cell (MMC) that undergoes an asymmetric cell division (ACD), producing a small meristemoid (M) and a large stomatal lineage ground cell (SLGC). Ms either differentiate into guard mother cells (GMCs) that divide symmetrically and form stomata or undergo several amplifying ACDs to produce additional SLGCs (12). The SLGCs can become pavement cells (PCs) or produce new satellite Ms as a result of a spacing ACD. All ACDs are strictly controlled by the activity of the transcription factor SPEECHLESS (SPCH). SPCH is negatively regulated by a canonical mitogen-activated protein kinase (MAPK) signaling module that functions downstream of a ternary receptor-peptide complex, including members of the ERECTA family (ERF), the receptor-like protein TOO MANY MOUTHS (TMM) and their ligands, the secreted cysteine-rich peptides, EPIDERMAL PATTERNING FACTORs (EPFs) (13). An intrinsic polarity complex, including the scaffolding proteins BREAKING OF ASYMMETRY IN THE STOMATAL LINEAGE (BASL), BREVIS RADIX-LIKE2 (BRXL2), and POLAR LOCALIZATION DURING ASYMMETRIC DIVISION AND REDISTRIBUTION (POLAR), is necessary for the ACD (14–17). BIN2 inhibits SPCH and the PM-localized MAPK components through phosphorylation and, consequently, limits or promotes stomatal development (8–10). These two BIN2 activities are regulated by the scaffolding function of POLAR that anchors BIN2 to the PM, attenuating the MAPK signaling and enabling SPCH to drive ACD in the nucleus (11). After ACD,

## Significance

Stomata, the gas exchange pores in plant epidermis, are formed by series of cell divisions and cell-fate transitions. Stomatal development is tightly controlled by endogenous and environmental cues. The BIN2 kinase, a key negative regulator of brassinosteroid signaling controls stomatal development, but the role of brassinosteroid hormones remains unclear. Here, through mapping the single-cell transcriptome of stomatal lineage in *Arabidopsis* after activation of brassinosteroid signaling with either exogenous hormones or the plant-specific BIN2 inhibitor, bikinin, we showed that the scaffold proteins POLAR and PL1 insulate BIN2 from brassinosteroid-mediated inactivation specifically in stomatal precursors. Our study reveals how different cell types interpret hormonal signals to initiate cell type-specific responses and correct cell patterning.

Copyright © 2023 the Author(s). Published by PNAS. This article is distributed under Creative Commons Attribution-NonCommercial-NoDerivatives License 4.0 (CC BY-NC-ND).

<sup>1</sup>E.-J.K., C.Z., B.G., and T.E. contributed equally to this work.

<sup>2</sup>Present address: Guangdong Provincial Key Laboratory of Plant Adaptation and Molecular Design, School of Life Sciences, Guangzhou University, Guangzhou 510006, China.

<sup>3</sup>Present address: Department of Plant Molecular Biology, University of Lausanne, Biophore, Lausanne 1015, Switzerland.

<sup>4</sup>Present address: Molecular Biology and Biotechnology, Council of Scientific & Industrial Research, National Botanical Research Institute, Lucknow 226001, India.

<sup>5</sup>To whom correspondence may be addressed. Email: beryb@psb.vib-ugent.be or eurus@psb.vib-ugent.be.

This article contains supporting information online at <https://www.pnas.org/lookup/suppl/doi:10.1073/pnas.2303758120/-DCSupplemental>.

Published August 28, 2023.

the reduced POLAR expression in the SLGC together with the inherited polarization of the phosphatase BSU1-LIKE1 (BSL1) leads to BIN2 accumulation in the nucleus, allowing the SLGC to differentiate into a PC (18). Despite recent knowledge on the function of BIN2 in stomatal development (8–11), the role of BRs in this process remains poorly understood (8, 9).

By generating and exploiting a high-resolution single-cell gene expression map of the stomatal lineage in *Arabidopsis*, we found that BR signaling activation by either exogenous BRs or the plant-specific BIN2 inhibitor, bikinin (19), triggered differential transcriptional responses with contrasting stomatal development outputs. Bikinin strongly suppressed stomata formation, whereas exogenous BRs induced ectopic divisions in stomatal lineage. We established that this opposite effect was due to different BIN2 inactivation modes; while exogenous BRs acted via the BRI1-dependent signal transduction pathway to inactivate BIN2 (1), the ATP-competitive inhibitor bikinin blocked it through a direct binding (19). When in a complex with POLAR and POLAR-LIKE1 (PL1) in the PM, BIN2 activity was insulated from the BR-mediated inactivation, but it remained sensitive to bikinin. Monitoring the dynamics of the BES1 nuclear accumulation in stomatal lineage revealed that the BR signaling is down-regulated in POLAR- and PL1-expressing ACD precursors, but that it is restored in SLGCs.

In summary, understanding the molecular basis that determines the contrasting effects of exogenous BRs and bikinin on stomatal lineage provided a mechanistic insight into an intrinsic developmental program regulation in which cell-specific responses are generated through scaffolding molecules. We showed that BR signaling attenuation achieved through scaffold-mediated insulation of BIN2 from inactivation by BRs preceded stomatal ACDs and it was required for stomatal patterning.

## Results

### Exogenous BRs and Bikinin Have Contrasting Effects on Cotyledon Epidermal Cells in *Arabidopsis*.

Pharmacological inhibition of BIN2 with bikinin (19) reduced stomatal density in the abaxial cotyledon and leaf epidermis of wild-type *Arabidopsis* and suppressed stomatal clustering in the *bin2-1* and *bsu-q* mutants (9). In contrast, wild-type plants grown on exogenous BRs did not exhibit any epidermal phenotypes in cotyledons (8, 20), which was difficult to reconcile with the BR signaling activation by both bikinin and BRs (4, 19). As BRs do not undergo long-distance transport (21) and treatments on agar media (8, 20) possibly limit the access of BRs to the above-ground tissues, wild-type *Arabidopsis* seeds were germinated and grown for 3 d in a liquid medium supplemented with increasing concentrations of either brassinolide (BL), the most active BR, or bikinin (*SI Appendix*, Fig. S1 A–E). None of treatments affected the cotyledon area at the highest concentrations (*SI Appendix*, Fig. S1A). However, exogenous BL significantly increased the total epidermal cell density in a concentration-dependent manner, because of an increased number of small ( $<200 \mu\text{m}^2$ ) nonstomatal cells as a result of additional cell divisions, whereas the stomatal index remained unaffected or slightly reduced at the highest BL concentration (*SI Appendix*, Fig. S1 B–E). In particular, the small ( $<200 \mu\text{m}^2$ ) nonstomatal epidermal cells retained a low degree of asymmetry after the division (*SI Appendix*, Fig. S1F), calculated according to the cell size of the daughter cells after division (11, 20). In contrast, and as previously reported (9), bikinin strongly reduced the total epidermal cell density, mainly due to a reduction in the small ( $<200 \mu\text{m}^2$ ) nonstomatal cell density and stomatal index (*SI Appendix*, Fig. S1 B–E). Altogether, these data indicate that exogenous BL and bikinin have an opposite impact on cotyledon epidermis, although they both activate BR signaling (19).

**BRs and Bikinin Trigger Spatiotemporally Distinct Transcriptional Responses.** To capture the differences between exogenous BL and bikinin at the cellular level, we applied single-cell transcriptomics of the stomatal lineage. First, a high-resolution single-cell RNA-seq map of stomatal lineage cells was generated as a control dataset (Fig. 1). For the profiling of stomatal lineage cells only, a fluorescence-activated cell sorting (FACS) was utilized on protoplast cells isolated from the aerial parts (cotyledons) of *Arabidopsis* seedlings that harbored the TMM reporters, *TMMpro:TMM-GFP* or *TMMpro:GFP* (22), 5 days post germination (dpg) (Fig. 1A). The *TMMpro:GFP* protoplasts were derived from a DMSO-treated tissue (mock control) for 2 h in liquid medium. After quality control (*SI Appendix*, Fig. S2 A and B) and stringent filtering steps (see *Materials and Methods* for details), we retained 8,005 and 4,937 individual high-quality cells from these two independent experiments with a minimum UMI count of 2,001 and 1,481 (Fig. 1B), respectively. Plotting the transcriptomes from the two datasets by means of the Uniform Manifold Approximation and Projection (UMAP) (23) revealed largely overlapping cell distributions between the translational and transcriptional TMM reporters used to generate these datasets, with the latter displaying a broader distribution range, consistent with its larger expression domain (Fig. 1A and B). Nine clusters reflecting the developmental transitions in the stomatal lineage were annotated with known stomatal markers (Fig. 1 C and D and Dataset S1) (24–28). Overall, the UMAP topology was similar to the previously published single-cell resolution map of the stomatal lineage (24, 26) with the exception of an additional cell cluster with unknown cell identity. To validate the predictions from our control dataset, we generated 21 reporter lines of previously unknown differentially expressed genes (DEGs) selected from each cell cluster. Except for two genes, *AT3G48520* and *AT4G04840* chosen as DEGs in the cluster “SLGCs and young PCs,” all examined reporter lines perfectly recapitulated the predicted expression domains (*SI Appendix*, Fig. S3), confirming the cluster annotation.

Next, we profiled sorted protoplasts derived from the aerial parts (cotyledons) of *Arabidopsis* seedlings expressing *TMMpro:GFP* at 5 dpg treated with BL (1  $\mu\text{M}$ ) and bikinin (50  $\mu\text{M}$ ) for 2 h in liquid medium without altering the expression pattern of TMM (*SI Appendix*, Fig. S2 C and D). After filtering for high-quality cells, 7,011 and 5,909 cells were retained from the BL- and bikinin-treated samples, respectively, with a minimum UMI count of 591 and 606 (Fig. 2A). The two datasets were then merged with the DMSO-treated *TMMpro:GFP* control sample, which was generated at the same time and the Seurat package was used to transfer cell annotation labels to the combined dataset (Fig. 2B). The three samples were interspersed across the UMAP plot (Fig. 2A) and contributed equally to each cell cluster (*SI Appendix*, Fig. S4A), suggesting that the new dataset provides a good predictive power and that it can be used for further analysis of the spatiotemporal gene expression during stomatal development.

To compare expression levels between treatments and across developmental transitions, we used the slingshot algorithm for trajectory inference (29), thus determining a pseudotime value for every cell (Fig. 2C). When the trajectory was mapped to the cell clusters, a dual trajectory emerged, one from Ms to young PCs (pseudotime 8 to 0) and one from Ms (pseudotime 8) through GMCs (pseudotime 12) to GCs (pseudotime 30). Thus, our dataset captured the entire developmental program of the stomatal lineage in pseudotime (Fig. 2C). Next, expression levels were calculated for each gene over the entire trajectory by means of the tradeSeq algorithm (30), resulting in expression profiles that can be compared between the different treatments for each

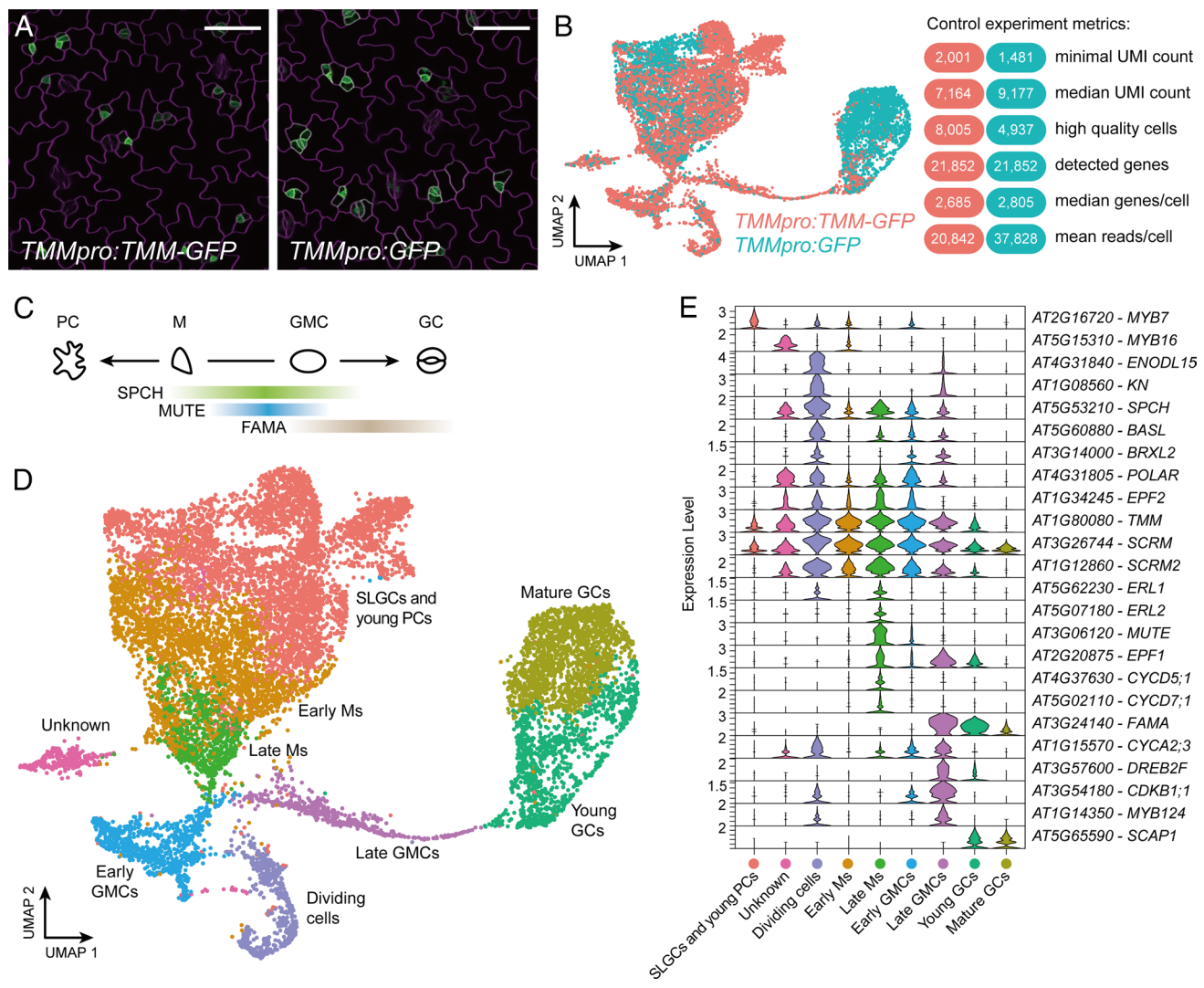


**Fig. 1.** Single-cell RNA sequencing of *Arabidopsis* stomatal lineage cells. (A) Confocal images of the abaxial cotyledon epidermis of plants expressing the translational (*TMMpro:TMM-GFP*) and transcriptional (*TMMpro:GFP*) TMM reporters at 5 dpg used for single-cell RNA sequencing (scRNA-seq). Cell outlines (magenta) were marked with propidium iodide. (Scale bars, 50  $\mu$ m.) (B) UMAP visualization of integrated scRNA-seq datasets derived from *TMMpro:TMM-GFP* and *TMMpro:GFP*. Each dot represents an individual cell. Cell transcriptomes generated from each individual experiment are indicated by different colors. (C) Schematic representation of stomatal development and expression levels shown by color intensity of three key stomatal regulators, the transcription factors SPCH, MUTE, and FAMA. (D) Color-coded UMAP plot showing the classification of single cells into nine distinct clusters corresponding to different cell identities in the stomatal lineage. M, meristemoid; SLGC, stomatal lineage ground cell; GMC, guard mother cell; GC, guard cell; PC, pavement cell. (E) Violin plots depicting level (height) and proportion of cell expression (width) of known stomatal lineage marker genes across each cell cluster. Colors correspond to cell clusters as shown in D.

developmental moment (see *Materials and Methods* for details) (Dataset S2). Then, we focused on genes with known functions in stomatal development that were predicted to be significantly differentially expressed along the pseudotime after BL or bikinin treatment (SI Appendix, Fig. S4 B–D and Dataset S2). BL mostly up-regulated stomatal markers expressed alongside the trajectory Ms-late Ms-early GMCs-late GMCs (Fig. 2D and SI Appendix, Fig. S4B), including *BASL*, *POLAR*, *EPF1*, *MUTE*, and the newly validated DEGs *AT5G11550* and *AT1G51405* for cluster “Early Ms” and “Late GMCs,” respectively (SI Appendix, Fig. S3 A and C). In contrast, bikinin either had no effect (*BASL*, *EPF1*, *MUTE*, *AT5G11550*, and *AT1G51405*) or down-regulated genes (*POLAR*, *EPF2*, *ERL1*, *CYCD7;1*, and the newly validated DEG for cluster “Early Ms” *AT3G62070*) in this trajectory (Fig. 2D and SI Appendix, Figs. S3 A and S4 B and C). Interestingly, bikinin up-regulated the GMC/GC marker genes, *SIAMESE-RELATED4* (*SMR4*) (31), *CYCLIN A2;3* (*CYCA2;3*) (28), and genes expressed in GCs, such as *AT3G47675* (SI Appendix,

Fig. S3D), *HIGH LEAF TEMPERATURE1* (*HT1*) (32) and *K<sup>+</sup> CHANNEL ARABIDOPSIS THALIANA2* (*KAT2*) (33) (SI Appendix, Fig. S4D). Quantitative real-time PCR analysis (qRT-PCR) of either wild-type seedlings or *TMMpro:GFP*-positive protoplasts isolated by FACS from seedlings treated with BL, bikinin, and DMSO as done for the scRNA-seq work (SI Appendix, Fig. S4 E and F), together with imaging and quantification of transcriptional reporters after similar treatments (SI Appendix, Fig. S4 G and H) validated the expression patterns of *POLAR*, *BASL*, *EPF2*, *MUTE*, *SMR4*, and *CYCA2;3*. In addition, long-term treatments also confirmed that exogenous BRs promoted the expression of stomatal regulators, whereas bikinin down-regulated them (Fig. 2 E and F and SI Appendix, Fig. S5).

Taken together, these results reveal that single-cell RNA sequencing is a powerful approach to detect spatiotemporally distinct transcriptional responses in stomatal lineage triggered by exogenous BL and bikinin, possibly the reason for the observed different epidermal phenotypes.

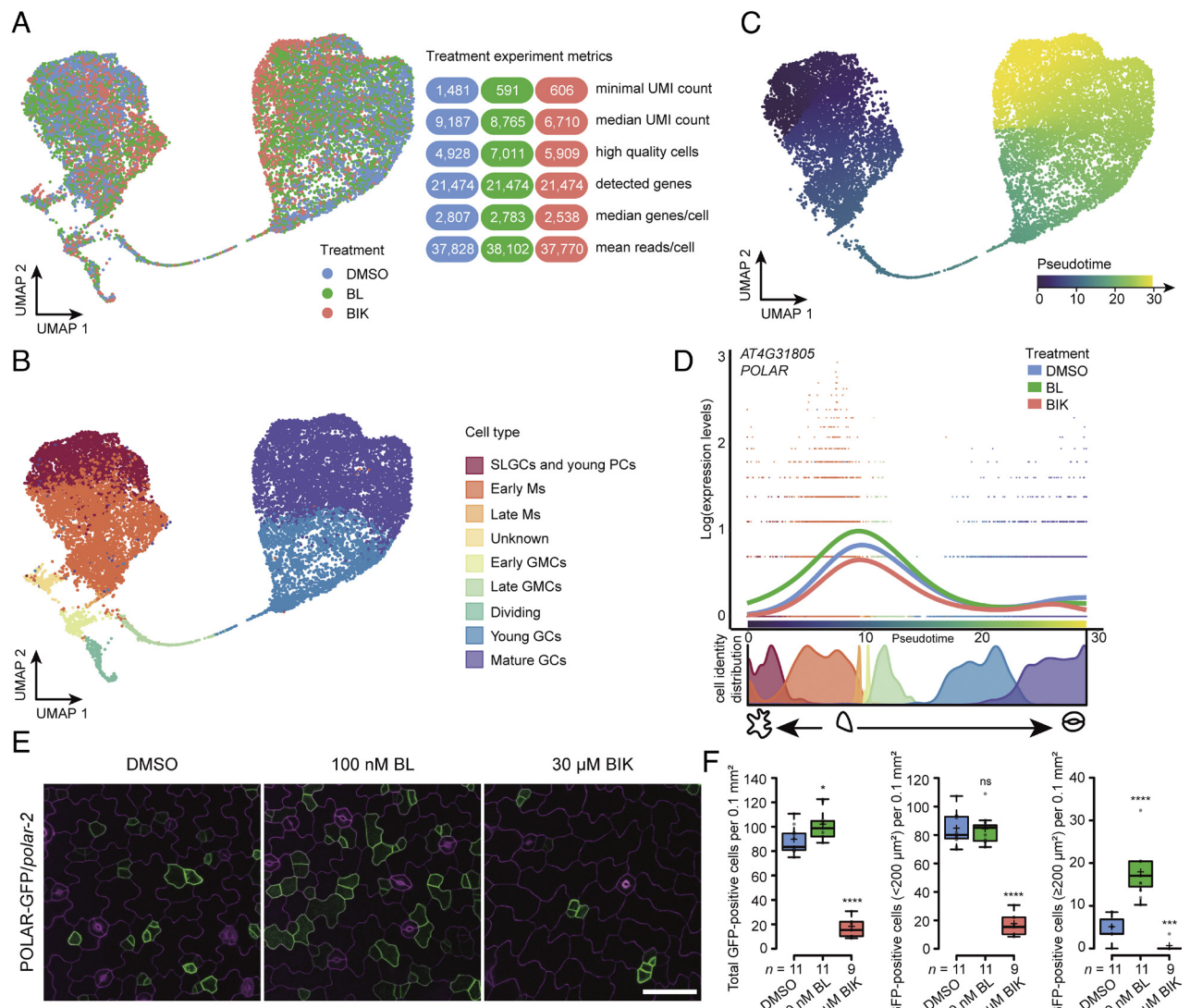


**Fig. 2.** BRs and bikinin trigger spatiotemporally distinct transcriptional responses. (A) UMAP visualization (Left) and experiment metrics (Right) of the integrated single-cell RNA sequencing datasets derived from the aerial parts (cotyledons) of seedlings at 5 dpg expressing *TMMpro:GFP* treated with brassinolide (BL, 1  $\mu$ M), bikinin (BIK, 50  $\mu$ M), and mock (DMSO) for 2 h in liquid medium. Each dot represents an individual cell. Cell transcriptomes are color-coded according to treatments. (B) UMAP plot of the merged data with indications of the cell type assignment. M, meristemoid; SLGC, stomatal lineage ground cell; GMC, guard mother cell; GC, guard cell; PC, pavement cell. (C) Color-coded pseudotime assignment for the merged data. (D) Expression trends of *POLAR* along pseudotime of the stomatal lineage trajectory after treatment with BL, BIK, and DMSO (Top) and distribution of the cell identities over the pseudotime trajectory, with colors denoting cell types as shown in B (Bottom). (E) Expression of *POLAR*-GFP [*POLARpro:gPOLAR-GFP/polar-2* (line #14.5)] in response to BL and BIK. Seeds were germinated and grown in liquid medium containing 100 nM BL, 30  $\mu$ M BIK, and DMSO (mock) for 3 d. Cell outlines (magenta) were marked with propidium iodide. (Scale bar, 50  $\mu$ m.) (F) Quantification of *E*. *POLAR*-GFP-positive cells per 0.1 mm<sup>2</sup>. Data points are plotted as dots. Center lines show the medians. Crosses represent sample means. Box limits indicate the 25th and 75th percentiles as determined by R software. Whiskers extend 1.5 times the interquartile range from the 25th and 75th percentiles. A single-factor ANOVA was used to determine significant differences between the mock control and treatments. \*\*\*P < 0.0001, \*\*P < 0.001, \*P < 0.05; ns, no significant difference. n, number of cotyledons analyzed.

### Constitutive Overexpression of *POLAR* and *PL1* Leads to BR Insensitivity.

When examining the list of genes with significant differential responses to bikinin and BL (Dataset S2), we noticed the known regulator of stomatal development and a direct interactor of BIN2, *POLAR* (11, 16). *POLAR* was up-regulated by BL and down-regulated by bikinin (Fig. 2 D–F and SI Appendix, Fig. S4 E and F). Consistent with the observed phenotypes (SI Appendix, Fig. S1) and the scRNA-seq data, bikinin suppressed the expression of *POLAR*-GFP in *POLARpro:gPOLAR-GFP/polar-2* (11), whereas exogenous BL prolonged the *POLAR*-GFP expression mostly in the SLGCs (Fig. 2 E and F). As *POLAR* functions redundantly with its closest homolog, *PL1* (At5g10890) (11, 25), we also examined the behavior of *PL1*-GFP (*PL1pro:gPL1-GFP/Col-0*) in the stomatal lineage (SI Appendix, Fig. S6). In the abaxial cotyledon epidermis of *Arabidopsis*, *PL1*-GFP polarized before the ACD in

a manner similar to that of *POLAR* (SI Appendix, Fig. S6 A and B and Movie S1). *PL1*-GFP copurified with mCherry-BASL, *POLAR*-mCherry, and *BIN2*-mCherry in tobacco (*Nicotiana benthamiana*) leaf epidermis (SI Appendix, Fig. S6C), and BASL-BFP efficiently polarized *PL1*-GFP, whereas the *PL1*-GFP expression alone lacked polarity (SI Appendix, Fig. S6 D and E). As previously reported for *POLAR* (11), in the presence of BASL, *PL1* excluded *BIN2* from the nucleus and subsequently tethered it to the PM in a polar fashion (SI Appendix, Fig. S6F). Moreover, long BL and bikinin treatments affected *POLAR* and *PL1* behavior similarly (Fig. 2 E and F and SI Appendix, Fig. S5D). Based on these findings, we hypothesized that *POLAR* and *PL1* probably function together and that they might, at least in part, be accountable for the differential responses to BL and bikinin observed in the stomatal lineage. In agreement, when treated

with BL, the sensitivity of the double *polar pl1* mutant (11) was significantly lower than that of the wild-type in terms of small ( $<200 \mu\text{m}^2$ ) nonstomatal cell density increase and large ( $>500 \mu\text{m}^2$ ) cell density decrease, whereas the impact of bikinin was equal to that of the wild-type (SI Appendix, Fig. S1 A, B, and F).

To further test our hypothesis, we generated transgenic lines expressing the genomic (g) fragments of POLAR and PL1 driven by the *CaMV 35S* promoter [*35Spro:gPOLAR* (POLAR-OE) and *35Spro:gPL1* (PL1-OE)] (Fig. 3 A and B and SI Appendix, Fig. S7A). Constitutive overexpression of either POLAR or PL1 in Arabidopsis resulted in an excess of small ( $<200 \mu\text{m}^2$ ) nonstomatal cells in the abaxial cotyledon epidermis at 3 dpg (SI Appendix, Fig. S7 B and C), but the phenotype was milder than that of POLAR, when overexpressed in its native domain (11). Moreover, these plants had more compact rosettes with dark-green and rounded leaves (Fig. 3 A and B), resembling a *bin2-1* mutant or plants overexpressing BIN2 (34), which are defective in BR signaling. Root growth inhibition assays with increasing BL concentrations revealed that all overexpression lines were insensitive to exogenous BRs (Fig. 3 C and D). In line with these observations,

overexpression of *POLAR* or *PL1* also increased the phosphorylated and total BES1 protein levels (Fig. 3 E and F). Consequently, BL treatment (100 nM) of *POLAR*-overexpressing plants did not induce BES1 dephosphorylation as efficiently as in the wild-type, even more prominently so with *PL1* overexpression (Fig. 3 E and F). In contrast, treatment with bikinin (50  $\mu\text{M}$ ) completely dephosphorylated BES1 in both overexpression lines, similarly to the wild-type (Fig. 3 E and F). Thus, when in a complex with *POLAR* or *PL1* the kinase activity of BIN2 was efficiently inhibited by bikinin, but not by BL. Nevertheless, BIN2 in a complex with either *POLAR* or *PL1*, was still able to phosphorylate BES1 without leading to its turnover. Overall, we conclude that BIN2, and possibly its homologs, do not undergo BR-mediated inactivation, but remain sensitive to bikinin when in a complex with *POLAR* and *PL1*.

### POLAR and PL1-Dependent Scaffolding of BIN2 Increases Its Stability and Activity.

To investigate the cause for the BR insensitivity of *POLAR* and *PL1*-overexpressing plants, we introduced each *35Spro:gPOLAR* or *35Spro:gPL1* construct into

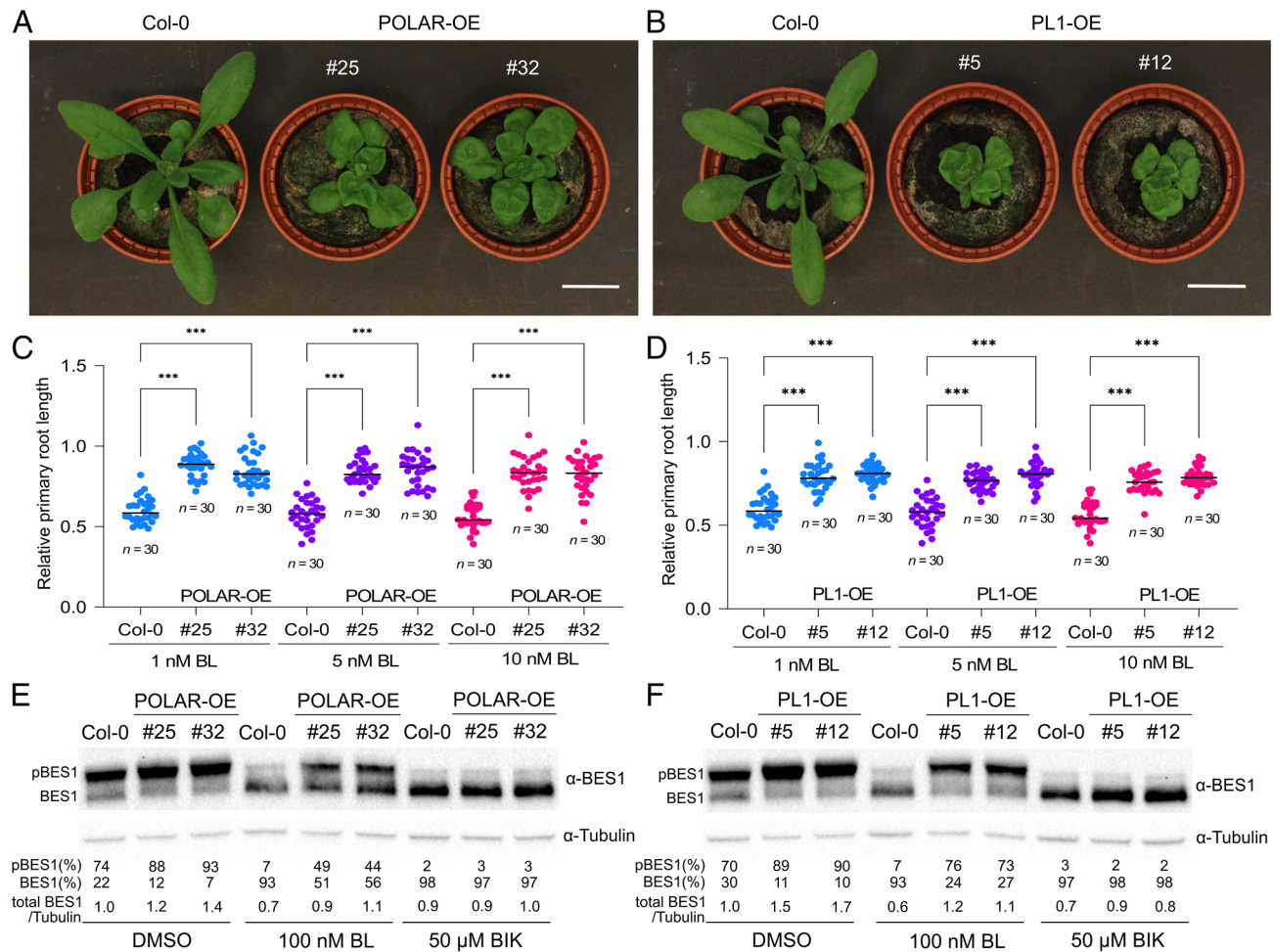


**Fig. 3.** Overexpression of *POLAR* and *POLAR-LIKE1* (*PL1*) led to BR insensitivity. (A and B) Phenotypes of 4-wk-old wild-type (Col-0) Arabidopsis and two independent homozygous transgenic lines overexpressing *POLAR* [*35Spro:gPOLAR* (POLAR-OE), lines #25 and #32] (A) and *PL1* [*35Spro:gPL1* (PL1-OE), lines #5 and #12] (B). (Scale bars, 2 cm.) (C and D) Root growth inhibition assay for testing BR sensitivity of Col-0, *POLAR*-OE (lines #25 and #32) (C), and *PL1*-OE (lines #5 and #12) (D) plants. Plants were grown in the presence of increasing concentrations of brassinolide (BL) (1 nM, 5 nM, and 10 nM) and DMSO (mock) for 5 d. The primary root length in the presence of BL is relative to the DMSO control. All individual data points are shown and black horizontal bars represent the means. *n*, number of roots analyzed. Two-way ANOVA with Tukey's multiple comparisons was used to determine significant differences between genotypes. \*\*\* $P < 0.0001$ . The data are representative of three independent experiments. (E and F) Endogenous BES1 levels in Col-0, *POLAR*-OE (lines #25 and #32) (E), and *PL1*-OE (lines #5 and #12) (F) plants after treatment with BL and bikinin (BIK). Five-day-old Arabidopsis seedlings were transferred to liquid media supplemented with 100 nM BL for 2 h or 50  $\mu\text{M}$  BIK for 1 h. BES1 was detected with  $\alpha$ -BES1 antibody and tubulin was used as a loading control and detected with  $\alpha$ -tubulin antibody. Quantification shows the ratio between phosphorylated (pBES1) and unphosphorylated BES1 (%). The total BES1 abundance is relative to the DMSO-treated control. The data are representative of three independent experiments.

the *BIN2pro:gBIN2-GFP/Col-0* (line #32.7) (11) ensuring that the BIN2-GFP levels remain the same (Fig. 4A and *SI Appendix*, Fig. S8 A and B). In parallel, we also transformed the *POLARpro:gPOLAR-mCherry* and *PL1pro:gPL1-mCherry* constructs into the same BIN2-GFP line [*BIN2pro:gBIN2-GFP/Col-0* (line #32.7)] (*SI Appendix*, Fig. S8 C–E). Examination of the abaxial cotyledon epidermis by confocal microscopy revealed a strong accumulation of the BIN2-GFP signal when either POLAR or PL1 were overexpressed (Fig. 4A and *SI Appendix*, Fig. S8 C and D). As previously reported for POLAR (11), overexpression of PL1 in its endogenous domain resulted in a strong overproduction of small stomatal lineage cells (*SI Appendix*, Fig. S8D). BIN2-GFP accumulated as a result of an overall increase in protein abundance because no changes in BIN2 transcripts were detected (*SI Appendix*, Fig. S8 B and E), as also confirmed by immunoblotting (Fig. 4B). Notably, BIN2 accumulation was higher in PL1-OE plants, consistent with the higher PL1 amounts, than that of POLAR in the POLAR-OE plants (Fig. 4B and *SI Appendix*, Fig. S8B), hinting at a dose-dependent effect. In line with the observed BIN2 stabilization in the presence of POLAR or PL1, BIN2 activity was also increased, as shown by immunoblot analysis with an  $\alpha$ -pTyr279-216-GSK3 $\alpha/\beta$  antibody recognizing the phosphorylated tyrosine in the activation loop of the animal GSK3 and frequently used to detect an active BIN2 in plants (Fig. 4B) (5). Subsequently, exogenous BL did not abolish BIN2 protein levels and kinase activity and did not completely dephosphorylate BES1 (Fig. 4B). Further nuclear fractionation experiments with BIN2-GFP-expressing

lines in the wild-type, POLAR-OE, and PL1-OE backgrounds revealed that the phosphorylated BES1 was more abundant in the cytoplasm of POLAR-OE or PL1-OE plants than that of the control (Fig. 4C). Exogenous BL fully dephosphorylated BES1 in the nucleus of BIN2-GFP plants, whereas the nuclear BES1 pool in POLAR-OE or PL1-OE plants was sensitive to BL, albeit to a lesser extent. The cytoplasmic pool of BES1 was reduced in the presence of BL in the control, whereas in the POLAR-OE or PL1-OE plants, BES1 remained insensitive to the hormone (Fig. 4C). Altogether, these observations prompted us to examine whether BES1 is recruited to the POLAR and PL1-BIN2 complex. Indeed, coimmunoprecipitation (Co-IP) assays in Arabidopsis (Fig. 4D) revealed that BES1 copurified with POLAR, PL1, and BIN2.

To explore whether POLAR or PL1 affected the BIN2 kinase activity through their direct interaction, we examined BIN2 auto-phosphorylation in vitro in the presence of POLAR or PL1 (Fig. 4E and *SI Appendix*, Fig. S8F). BIN2 kinase activity increased in the presence of POLAR or PL1, but more importantly when the two scaffolds were added simultaneously. Collectively, we show that when in a complex with POLAR and PL1, BIN2 is stabilized and its kinase activity is increased, consequently leading to BR insensitivity.

**BR Signaling Is Attenuated in ACD Precursors.** Given that POLAR and PL1 are exclusively expressed in the early stomatal lineage (*SI Appendix*, Fig. S6 A and B and Movie S1) (11, 16, 25), we assumed that BIN2 protection from BR-mediated inactivation in these cells is important for stomatal development. To gain

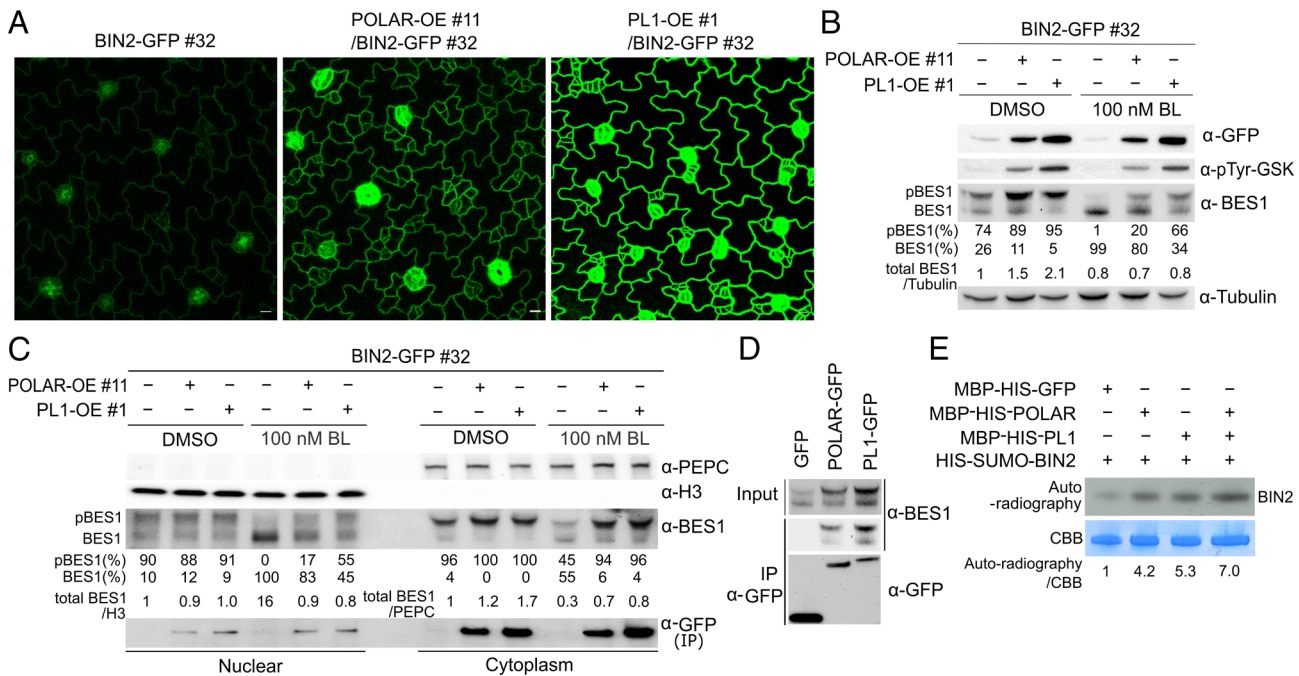


**Fig. 4.** POLAR and PL1 scaffolding of BIN2 increased its stability and activity. (A) Abaxial cotyledon epidermis of Arabidopsis seedlings at 3 dpg expressing BIN2-GFP in wild-type [*BIN2pro:gBIN2-GFP/Col-0* (line #32.7)] and in plants overexpressing (OE) either POLAR [*POLAR-OE* (line #11), *35Spro:gPOLAR/BIN2pro:gBIN2-GFP* (line #32.7)/*Col-0*] or PL1 [*PL1-OE* (line #1), *35Spro:gPL1/BIN2pro:gBIN2-GFP* (line #32.7)/*Col-0*]. (Scale bars, 20  $\mu$ m.) (B) BIN2-GFP protein levels in plants in (A) treated with 100 nM brassinolide (BL) and DMSO (mock) for 1 h in liquid medium. BIN2-GFP was captured by immunoprecipitation and detected with  $\alpha$ -GFP and  $\alpha$ -pTyr-GSK antibodies. Tubulin was used as a loading control and detected with  $\alpha$ -tubulin antibody. BES1 was detected with  $\alpha$ -BES1 antibodies. Quantification of the ratio unphosphorylated/phosphorylated (p)BES1 indicated in %. The total BES1 abundance is relative to the DMSO-treated BIN2-GFP control. (C) Nuclear fractionation of plants in (A) treated as in (B). Phosphoenolpyruvate carboxylase (PEPC) and histone H3 (H3) were used as cytosolic and nuclear markers, respectively. BIN2-GFP was detected after immunoprecipitation (IP) with  $\alpha$ -GFP antibody. BES1 was detected with  $\alpha$ -BES1 antibody. The blot is labeled as in (B). The total BES1 protein was quantified relative to H3 and to PEPC. (D) BES1 copurified with POLAR-GFP and PL1-GFP in Arabidopsis seedlings at 3 dpg. Transgenic POLAR-GFP-OE [*35Spro:gPOLAR-GFP/Col-0* (line #3.1)], PL1-GFP-OE [*35Spro:gPL1-GFP/Col-0* (line #1.6)], and GFP-OE [*35Spro:GFP/Col-0*] plants were used. GFP-OE was used as a negative control. The  $\alpha$ -GFP antibody was used for immunoprecipitation and  $\alpha$ -GFP and  $\alpha$ -BES1 for detection. (E) In vitro autophosphorylation assay of BIN2 in the presence of POLAR and PL1. SUMO-HIS-BIN2 was incubated with MBP bead-bound MBP-HIS-GFP, MBP-HIS-POLAR, and MBP-HIS-PL1. After a reaction with  $^{32}$ P- $\gamma$ -ATP for 2 h at 30 °C, only the supernatant fraction containing SUMO-HIS-BIN2 of each sample was collected and separated by SDS-PAGE. Autoradiography signal shows kinase activity. Quantification indicates the autophosphorylation activity of SUMO-HIS-BIN2 relative to its protein level. CBB, Coomassie Brilliant Blue.

more insight into the BR signaling regulation in stomatal lineage, we analyzed the BES1-GFP (35) localization in the abaxial cotyledon epidermis of wild-type *Arabidopsis* plants expressing *BES1pro:gBES1-GFP* (34) and the PM marker *ML1pro:mCherry-RCI2A* (36) at 2 dpg (Fig. 5A). BES1-GFP was ubiquitously expressed throughout the cotyledon epidermis but displayed

differences in its nuclear localization in the stomatal lineage. BES1-GFP was enriched in the nuclei of SLGCs or PCs but was less abundant in MMCs or Ms (Fig. 5A), consistent with the observed enhanced PM association of BIN2 and its homologs in these cells (11). A time-lapse imaging was performed over a 9-h course to track BES1-GFP before and after the amplifying ACD

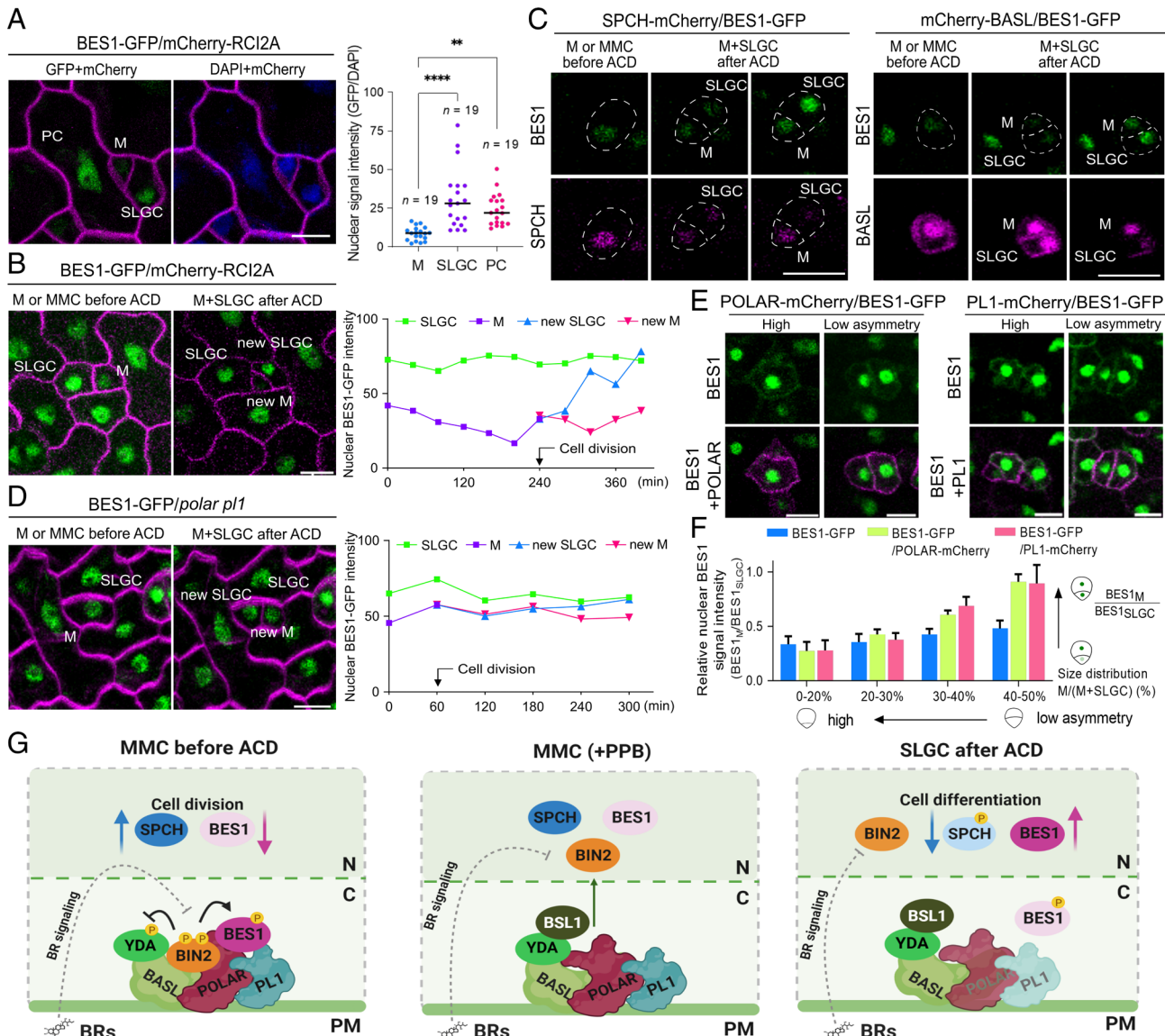


**Fig. 5.** BR signaling is attenuated in ACD precursors. (A) Localization of BES1-GFP (*BES1pro:gBES1-GFP/ML1pro:mCherry-RCI2A/Col-0*) in stomatal lineage in the abaxial cotyledon epidermis. Quantification shows the nuclear intensity of BES1-GFP normalized to DAPI, in M, SLGC, and PC. All individual data points are shown and black horizontal bars represent the means. One-way ANOVA and Dunnett's multiple comparison tests were used to determine significant differences between Ms and each SLGC and PC. \*\*\*P < 0.0001, \*\*P < 0.01. n, number of cells analyzed. (B) Expression pattern of BES1-GFP before and after ACD. The nuclear BES1-GFP intensity was quantified over time as indicated. Arrow marks the time point of cell division. (C) Expression pattern of BES1-GFP combined with either SPCH-mCherry [*SPCHpro:gSPCH-mCherry/BES1pro:gBES1-GFP* (line #5)] or mCherry-BASL [*BASLpro:mCherry-gBASL/BES1pro:gBES1-GFP* (line #9)] in stomatal lineage before and after ACD. Cell outlines were marked by dashed lines. (D) Expression pattern of BES1-GFP in the *polar p1* mutant [*BES1pro:gBES1-GFP/polar p1* (line #11)] before and after ACD. The nuclear BES1-GFP intensity was quantified over time as indicated. Arrow marks the time point of cell division. (E) Expression pattern of BES1-GFP in POLAR-OE [*POLARpro:gPOLAR-mCherry/BES1pro:gBES1-GFP/Col-0* (line #3)] and PL1-OE [*PL1pro:gPL1-mCherry/BES1pro:gBES1-GFP/Col-0* (line #2)]. The representative images show the BES1-GFP expression in the cells with different degrees of asymmetry between Ms and SLGCs after cell division. (F) Quantification of the nuclear BES1-GFP intensity in plants described in E. The nuclear BES1-GFP intensity of M compared to SLGC was measured as a relative value and presented according to the size distribution between Ms and SLGCs. From each genotype, 100 Ms and 100 SLGCs were analyzed. Error bars represent SD. The abaxial cotyledon epidermis was examined at 2 dpg (B–D) and 3 dpg (A and E). [Scale bars, 10 μm (A–E).] (G) Working model for the BIN2 insulation from BR-mediated inactivation by POLAR and PL1 during stomatal ACD. In the MMC or M, in which POLAR and PL1 are highly expressed before the ACD, BIN2 is recruited to the plasma membrane (PM) together with BASL, POLAR, and PL1. In this complex, BIN2 remains active, insensitive to BR-mediated inhibition and inactivates YODA (YDA) through phosphorylation. As a result, the high activity of SPCH in the nucleus promotes ACD. BES1 is associated with POLAR and PL1 near the PM and remains phosphorylated by BIN2, thus suppressing BR signaling. During cell division, when the preprophase band (PPB) is formed, the phosphatase BSL1 associates with the BASL polarity complex and mediates BIN2 dissociation from the PM. After ACD, a reduction of POLAR and PL1 expression promotes BIN2 repartitioning to the nucleus; as a consequence, YDA in the PM is activated causing a strong suppression of the SPCH activity, which restricts ACD. In parallel, BIN2 is accessible for BR-mediated inactivation. Hence, dephosphorylated BES1 is then translocated into the nucleus to activate BR responses followed by pavement cell differentiation. The figure was created with BioRender (BioRender.com).

(Fig. 5B and Movie S2). Before the ACD, the nuclear BES1-GFP signal in Ms decreased, but after division, it increased in the nucleus of SLGCs, while remaining low in the nucleus of the newly formed Ms, albeit reaching the same expression levels as before the ACD (Fig. 5B). Examination of the colocalization of BES1-GFP (*BES1pro:gBES1-GFP/Col-0*) with SPCH-mCherry (*SPCHpro:gSPCH-mCherry/Col-0*) and mCherry-BASL (*BASLpro:mCherry-gBASL/Col-0*) before and after ACDs (Fig. 5C) revealed that, as anticipated, the BES1-GFP signal was strongly reduced in Ms with highly expressed SPCH and polarized BASL at the cell cortex before division (Fig. 5C). In contrast, the nuclear signal of BES1-GFP in the *polar pl1* double mutant remained enriched in Ms before and after the amplifying ACD (Fig. 5D and SI Appendix, Fig. S9 A and B). Because the nuclear accumulation of BES1-GFP is routinely used as a readout for active BR signaling (3), our data suggest a BR signaling attenuation in ACD precursors. This conclusion was further substantiated by the observed elevated expression in Ms of the BR biosynthetic enzymes, DWF4-GFP (*DWF4pro:DWF4-GFP/dwf4*) (21) and GFP-BR6OX2 (*BR6OX2pro:GFP-BR6OX2/br6ox1 br6ox2*) (21) of which a feedback inhibition via the BR signaling is known (SI Appendix, Fig. S9C) (37). This supports the notion that the BR signaling is down-regulated in ACD precursors as a consequence of BIN2 insulation from BR inactivation by POLAR and PL1.

We next investigated whether manipulation of endogenous BR signaling would impact epidermal development. To that aim, we analyzed the abaxial cotyledon epidermis of plants deficient in BR-induced responses due to the simultaneous inactivation of BES1 and its four homologs, designated as the *bzr-quintuple* [(*bzr-qui*, *bes1 bzr1 beh1 beh3 beh4*] mutant (38), along with *bes1-D* plants carrying a gain-of-function mutation in BES1 that results in constitutive BR responses (3). When compared to the wild-type, *bzr-qui* had increased total epidermal cell densities, while *bes1-D* showed opposite phenotypes but in both cases the stomatal index remained unaffected at 12 dpg (SI Appendix, Fig. S9 D–F). In agreement, a careful examination of the epidermis established that the *bzr-qui* at 3 dpg had an increased number of epidermal cells with sizes between 100 and 500  $\mu\text{m}^2$  corresponding to SLGCs and young PCs, while the number of Ms and GMCs with size  $<100 \mu\text{m}^2$  was not changed (SI Appendix, Fig. S9G). On the contrary, constitutive BR signaling caused by the stabilized BES1 variant reduced the epidermal cell divisions and promoted cell differentiation (SI Appendix, Fig. S9 D–F). As such, we conclude that although attenuation of BR responses per se was not sufficient to induce additional ACDs resulting in more Ms and, hence, stomata, it triggered ectopic epidermal cell divisions in SLGCs and young PCs.

The scRNA-seq data and validation revealed that exogenous BRs up-regulate the expression of early stomatal regulators, consistent with the known stabilization of the SPCH protein by BRs (8) that results in ectopic epidermal cell divisions, a phenotype similar to that of overexpressing POLAR and PL1 in their native domains (SI Appendix, Fig. S8 C and D). To assess the BES1-GFP nuclear localization in these overexpression lines, we introduced *POLARpro:gPOLAR-mCherry* and *PL1pro:gPL1-mCherry* constructs into the *BES1pro:gBES1-GFP/Col-0* plants (Fig. 5 E and F and SI Appendix, Fig. S9 H and I). Nuclear BES1-GFP intensity was classified according to the cell size after division (11, 20). As previously reported for POLAR-GFP (11), overexpression of PL1-GFP also reduced the asymmetry in the cell clusters because most of the cells produced from divisions of Ms had similar sizes (SI Appendix, Fig. S9H). BES1-GFP had different fluorescence intensities depending on the level of cellular asymmetry after division when either POLAR or PL1 was overexpressed (Fig. 5F). BES1-GFP was strongly reduced in small cells with a high degree

of asymmetry, whereas in cells with low asymmetry levels BES1 was more abundant and clearly enriched in the cytoplasm near the PM (Fig. 5 E and F and SI Appendix, Fig. S9H). Regardless of the level of cellular asymmetry, POLAR or PL1 overexpression resulted in accumulation of BES1-GFP in the cytoplasm (SI Appendix, Fig. S9I). As the stomatal index did not increase in the POLAR-overexpressing plants (11), we conclude that cells with increased nuclear BES1 accumulation will probably acquire a PC fate. In summary, exogenous BRs or overexpression of the scaffolds POLAR and PL1 in the stomatal lineage trigger ectopic cell division as a result of alleviating SPCH inhibition by BIN2 and MAPK signaling in Ms and SLGCs.

## Discussion

Understanding how different cell types interpret plant hormones to initiate cell type-specific responses remains a major challenge in plant developmental biology. Here, identification of the molecular mechanism behind the different effects of exogenous BR signaling activators (BL and bikinin) on stomatal lineages combined with single-cell transcriptomics and live imaging revealed the mechanistic framework underlying the involvement of BRs in the induction of stomatal ACDs. The role of BRs in stomatal development has long been a subject of debate because both negative (9, 10) and positive effects (8, 20, 39) have been reported. Interestingly, a negative role relied mostly on the use of the small-molecule bikinin (19). Indeed, bikinin treatment suppressed divisions in stomatal lineage, whereas exogenous BRs promoted them. Although bikinin activates BR responses similarly as BRs and its application phenocopies plants with constitutive BR responses, some genes, including stomatal regulators, have been reported to be controlled in an opposite manner (19). These dissimilarities might lie in the different BIN2 inhibition mode. Whereas bikinin acts directly at the BIN2 level (19), BRs function through a signaling pathway mediated by protein-protein interactions (1). Hence, we hypothesized that the BR-mediated BIN2 inactivation is regulated differently in stomatal lineages. This concept was further confirmed by sequencing the transcriptome of individual cells in stomatal lineages and by identifying the behavior of each stomatal lineage cell type after treatment with either BL or bikinin. The pseudotime analysis revealed that most of the early stomatal lineage genes (*BASL*, *POLAR*, *EPF1*, and *MUTE*) along the Ms-to-GCs trajectory are up-regulated by BRs, whereas they are either not affected (*BASL*, *EPF1*, and *MUTE*) or suppressed (*POLAR*, *EPF2*, *CYCD7;1*, and *ERL1*) by bikinin. Interestingly, bikinin up-regulated the cyclin-dependent kinase inhibitor *SMR4* that was recently reported to repress ACDs through inhibition of the activity of *CYCD7;1* (31), which is specifically expressed just prior to the symmetric GC-forming division (40). Given that expression of key stomatal regulators, such as *POLAR*, *PL1*, *BASL*, and *MUTE* are induced by SPCH (15), the prolonged expression of POLAR and PL1 in stomatal lineage caused by exogenous BRs implies that BR-induced ectopic cell divisions are triggered by SPCH stabilization (8). Indeed SPCH protein levels were up-regulated by BRs (8) and down-regulated by bikinin (SI Appendix, Fig. S5A). In view of the broader SPCH expression in stomatal lineage (23), BRs probably stabilize SPCH not only in Ms but also in SLGCs and/or GCs. Therefore, the cell divisions induced by BRs might not all result in stomata. Exogenous BRs reduced the asymmetry of the cell divisions in a manner similar to that by overexpression of POLAR, which did not increase the stomatal index (11). Thus, exogenous BRs positively regulate epidermal cell divisions, possibly through SPCH stabilization and consecutive upregulation of POLAR and PL1 that additionally reinforced the SPCH activity through BIN2 scaffolding.

Previously, POLAR had been shown to not only polarize but also to enhance the PM association of BIN2 and its homologs in ACD precursors (11). The PM scaffolding of BIN2 by POLAR resulted in alleviation of the SPCH inhibition by BIN2 and MAPK, followed by ACD induction (8–11). A similar scaffolding mechanism for BIN2 was described in the protophloem of the Arabidopsis root, in which OCTOPUS (OPS) recruits BIN2 to the PM, thus preventing its inhibitory activity in the nucleus. Overexpression of OPS led to constitutive BR responses (41) but overexpression of POLAR and PL1 caused BR insensitivity, while retaining sensitivity to bikinin. The BR resistance was caused by an increased BIN2 protein stability and kinase activity. Thus, when in a complex with POLAR and PL1, BIN2 is protected from BR-mediated inactivation and degradation via a still unknown mechanism. Moreover, the PM-recruited and stabilized BIN2 remained active and accumulated phosphorylated BES1 in the cytoplasm, therefore restraining the BR signaling. The accumulation of dephosphorylated BES1 is used as a proxy for BR signaling activation (21, 35). Analysis in the wild type revealed a strong reduction of the nuclear BES1 accumulation in ACD precursors, whereas the nuclear BES1-GFP was enriched in SLGCs and PCs, suggesting that downregulation of BR signaling in Ms precedes ACD. In contrast, BR signaling was enhanced in SLGCs and PCs probably to ensure differentiation. It has been shown recently that BR signaling controls PC shape by activating ROP2 signaling preferentially in the lobes (42). Interestingly, the *bzr-quui* mutant, which is deficient in BR-induced responses (38), had an increased number of small epidermal cells that by size corresponded to SLGCs and young PCs. Therefore, deficiency in BR-induced responses led to ectopic cell divisions in SLGCs likely as a result of increased BR production due to lack of feedback regulation and possibly SPCH stabilization in cells expressing POLAR and PL1. In addition, impaired functions of BES1 and its homologs precluded cell differentiation of SLGCs. Correspondingly, *bes1-D* plants had fewer epidermal cells that were larger than those of the wild-type.

Taken together, we propose a model (Fig. 5G and *SI Appendix*, Fig. S10A), in which BIN2 is recruited to the PM by POLAR and PL1 in ACD precursors. Consequently, BIN2 is stabilized, hyperactive, and protected from BR-mediated inactivation by the POLAR and PL1 interaction. As a result, BR signaling in ACD precursors is attenuated to allow cell division via SPCH and to preclude cell differentiation. However, exogenous bikinin inactivates BIN2 regardless of the scaffolds. Hence, the MAPK signaling module remains active and inhibits the ACD through inactivation of SPCH. Recently, a polarization of the phosphatase BSL1 in stomatal ACD precursors was shown to be triggered at the onset of mitosis (18). Polarized BSL1 is then inherited by the differentiating SLGCs, where it suppresses cell division and promotes cell-fate determination through BIN2 repartitioning to the nucleus. This model is in agreement with our observations that post ACD in SLGCs, and in the absence of POLAR and PL1 expression, BIN2 is inactivated by BRs to permit cell differentiation coinciding with a nuclear increase of BES1. In summary, our work reveals that BR signaling controlled through BIN2 interaction with scaffolding proteins ensures the correct stomatal patterning in the leaf epidermis. We believe that these findings will contribute to a better understanding of water loss and gas exchange in plants, which is crucial for improving plant resilience in the face of climate change.

## Materials and Methods

**Plant Materials and Growth Conditions.** Seeds of *Arabidopsis thaliana* (L.) Heynh. Columbia-0 (Col-0) and of the described genotypes sown on half-strength Murashige and Skoog (1/2MS) agar plates or in liquid 1/2MS medium

without sucrose were stratified for 2 d in the dark at 4 °C. The seeds were germinated and grown at 22 °C and under a 16-h light/8-h dark photoperiod for 3, 5, or 7 d, according to the experimental purposes. When indicated, brassinolide (BL) (OIChemIm, Ltd.) or bikinin (home synthesized) were added to the medium at a final concentration of 1, 5, 10, or 100 nM for BL, and 10, 30, or 50 μM for bikinin. The following transgenic Arabidopsis lines or mutants have been described previously: *TMMpro:TMM-GFP/Col g1-1*, *TMMpro:GUS-GFP/Col g1-1* (22), *ML1pro:mCherry-RCI2A/Col-0* (36), *POLARpro:gPOLAR-GFP/polar*, *BIN2pro:gBIN2-GFP/Col-0*, *POLARpro:gPOLAR-mCherry/BIN2pro:gBIN2-GFP*, and *polar pl1* (11), *SPCHpro:SPCH-GFP/spch-3* (8), *BES1pro:BES1-GFP/Col-0* (35), *EPF1pro:erGFP/Col-0* (43), *MUTEpro:MUTE-GFP/mute* (44), *MUTEpro:GFP-GUS* (45), *FAMApro:FAMA-GFP/Col-0* (46), *SMR4pro:GFP-GUS/Col-0* (47), and *bes1 bzr1 beh1 beh3 beh4 (bzr-quui)* (38). The *bes1-D* (3) was backcrossed with Col-0 to remove the En2 background. For the phenotypic analysis of 4-wk-old Arabidopsis plants, 7-d-old seedlings grown in 1/2MS plates were transferred to soil and were grown at 21 °C under a 16-h light/8-h dark regime. Wild-type tobacco (*Nicotiana benthamiana*) plants were grown in the greenhouse at 25 °C under a normal light regime (14 h light/10 h dark). For the single-cell sequencing experiment, Arabidopsis plants of *TMMpro:TMM-GFP/Col g1-1* and *TMMpro:GUS-GFP/Col g1-1* were grown vertically on solid 1/2MS plates without sucrose under continuous 24 h light conditions for 5 d.

**Generation of Constructs and Transgenic Lines.** The transcriptional or translational reporter constructs for validating the cell cluster annotation of the single-cell sequencing are listed in *SI Appendix, Table S1*. For *AT5G11550*, *AT2G41190*, *AT1G75900*, *AT1G04110*, *AT1G51405*, *AT4G04840*, and *AT3G08770*, the promoter region (up to ~3 kb) and the full-length genomic fragment of each gene were recombined with GFP into pB7m34GW by means of the Gateway LR clonase enzyme mix (Thermo Fisher Scientific). The other expression constructs were generated via Golden Gate assembly (NEB). The promoter region (up to ~3 kb) upstream of the transcriptional start was cloned into the pGGA000 entry vector, whereas the full-length genomic coding region was cloned into the pGGC000 entry vector (48). For translational reporter constructs, entry clones bearing the promoter, the genomic coding region, or GFP were recombined into the final expression vector pFASTRK-AG (49). For transcriptional reporter constructs, entry modules carrying the promoter region, a nuclear localization signal linker, or GFP were cloned into pGGB-AG (48). The protocol for Golden Gate assembly has been described previously (49). Of each entry plasmid 100 ng was combined with 1× Cutsmart buffer (NEB), 1 mM ATP, 10 units of BsAl (NEB), and 200 units of T4 DNA ligase (NEB). The Golden Gate assembly reaction was carried out under the following conditions: 20 cycles at 37 °C for 2 min followed by 2 min at 16 °C, 5 min at 50 °C, and 5 min at 80 °C. The constructs were transformed into Col-0 or *ML1pro:mCherry-RCI2A*-expressing plants.

For *UBQ10pro:PIP2A-mCherry*, the coding sequence of *PLASMA MEMBRANE INTRINSIC PROTEIN 2A (PIP2A)* was cloned into *pENTR/D-TOPO* and was subsequently recombined with *pDONR-p4p1r-UBQ10pro* and *pDONR-p2p3-mCherry* into *pH7m34GW*. *pDONR-p2p3-BASL* (11) was recombined with *pDONR-p4p1r-BASLpro* (11) and *pDONR221-GFP* into *pH7m34GW* to generate *BASLpro:GFP-BASL*. The expression cassette of *UBQ10pro:PIP2A-mCherry* was then recombined with *BASLpro:GFP-BASL* by means of the Gibson assembly to generate the *BASLpro:GFP-BASL-UBQ10pro:PIP2A-mCherry* construct, which was transformed into Col-0 plants. To generate the *pEPF2pro:EPF2-GFP* construct, the *EPF2* genomic fragment containing 1,737 bp of the promoter, three exons, and two introns was amplified by PCR and recombined into the *pK7FWG* construct. The construct was subsequently transformed into Col-0 plants. For *POLAR-LIKE1 (PL1)*, the genomic fragment containing 1,766 bp of the promoter, two exons, and one intron was cloned into *pDONR-p4p1r* and recombined with *pDONR221-mCherry* or *pDONR221-GFP* into the *pB7m24GW;3* vector to generate the *PL1pro:gPL1-mCherry* or *PL1pro:gPL1-GFP* constructs, which were transformed into *BIN2pro:gBIN2-GFP/Col-0* (11) and Col-0 plants to generate *PL1pro:gPL1-mCherry/BIN2pro:gBIN2-GFP/Col-0* and *PL1pro:gPL1-GFP/Col-0* transgenic plants, respectively. The *PL1pro:gPL1-mCherry* construct and the previously described constructs, including *POLARpro:gPOLAR-mCherry*, *SPCHpro:SPCH-mCherry*, and *BASLpro:mCherry-gBASL* (11) were transformed into *BES1pro:gBES1-GFP/Col-0* plants (34). The genomic fragment of *BES1* containing 1,563 bp of the promoter, three exons, and two introns was cloned into *pDONR-p4p1r* and recombined with *pDONR221-GFP* into the *pH7m24GW;3* vector to generate the

*BES1pro:gBES1-GFP* construct. The construct was subsequently transformed into Col-0 and *polar* *pl* plants (11). For the generation of overexpression lines, genomic DNA (gDNA) of *PL1* was cloned into *pDONR221*. gDNA of *PL1* and *POLAR* (11) were recombined into the pK7WG2 vector containing the *Cauliflower mosaic virus* (*CaMV*) 35S promoter, of which the resulting constructs were transformed into Col-0 and *BIN2pro:gBIN2-GFP/Col-0* (11), respectively. For transient expression in tobacco, the 35Spro:*BIN2-GFP*, 35Spro:*TagBFP2-BASL*, 35Spro:*mCherry-BASL*, and 35Spro:*POLAR-mCherry* constructs had been described previously (11). cDNA of *PL1* was cloned into *pDONR221* and recombined in pK7FWG2 containing the 35S promoter and the C-terminal *GFP*-coding sequence to generate the construct 35Spro:*PL1-GFP*. The *BIN2* cDNA (11) was recombined with the 35S promoter and *mCherry* into the pb7m34GW vector to generate 35Spro:*BIN2-mCherry*.

For the purification of MBP-HIS-POLAR, MBP-HIS-*PL1*, MBP-HIS-*GFP*, and SUMO-HIS-*BIN2* proteins in *Escherichia coli*, cDNA of *POLAR*, *PL1*, or *GFP* were recombined into the *pDEST-HIS-MBP* vector. cDNA of *BIN2* was recombined into the *pET-SUMO-SH* vector. All primers used for cloning are listed in *SI Appendix*, Table S2.

**Chemical Treatments.** For the single-cell sequencing experiment, 5 dpg, Arabidopsis seedlings expressing *TMMpro:GUS-GFP* were immersed in liquid ½MS medium supplemented with 1 µM BL, 50 µM bikinin, or 0.1% (v/v) DMSO for 2 h. For the analysis of the effect of BL and bikinin on the abaxial cotyledon epidermis of Arabidopsis seedlings, seeds were directly germinated and grown for 3 d in liquid ½MS supplemented with the indicated concentration of BL or bikinin. For the BES1 phosphorylation assay upon BL or bikinin treatment, Arabidopsis seedlings of Col-0, 35Spro:*gPOLAR/Col-0*, or 35Spro:*gPL1/Col-0* were germinated and grown on ½MS plates for 5 d and then transferred to liquid ½MS for 2 h and supplemented with DMSO, 100 nM BL, or 50 µM bikinin for 1 h. For the root inhibition assay upon BL or bikinin treatment, Col-0, 35Spro:*POLAR/Col-0*, or 35Spro:*gPL1/Col-0* were germinated and grown on ½MS plates containing 0, 1, 5, or 10 nM BL for 5 d. For the nuclear and cytoplasmic BES1 fractionation assay, 35Spro:*gPOLAR/BIN2pro:gBIN2-GFP/Col-0*, 35Spro:*gPL1/BIN2pro:gBIN2-GFP/Col-0*, and *BIN2pro:gBIN2-GFP/Col-0* were grown on ½MS agar plates for 3 d and then transferred to liquid ½MS containing DMSO or 100 nM BL for 1 h.

**Single-Cell Sample Preparation, Library Construction, and Sequencing.** Protoplasts were isolated as described previously (50) with minor modifications. Briefly, the whole aerial tissue of the Arabidopsis seedlings was harvested and incubated in protoplasting solution [1.5% (w/v) cellulase Y-C, 0.15% (w/v) pectolyase Y-23, 0.4 M mannitol, 20 mM KCl, 10 mM CaCl<sub>2</sub>, 0.1% (w/v) bovine serum albumin (BSA), 20 mM MES, pH 5.7]. After 1 h of gentle shaking, cells were filtered through a 70-µm cell strainer and spun down at 100g for 6 min. Pelleted protoplasts were resuspended with washing solution [0.4 M mannitol, 20 mM KCl, 10 mM CaCl<sub>2</sub>, 0.1% (w/v) BSA, 20 mM MES, pH 5.7] and filtered through a 40-µm cell strainer. The protoplasts were then sorted on a FACSaria II (BD Biosciences) based on the GFP signal. Sorted cells were centrifuged at 400g at 4 °C for 5 min and resuspended in a washing solution to yield an estimated concentration of 1,000 cells/µL. Cellular suspensions were loaded on either a GemCode Single Cell 3' Gel Bead and Library Kit (V2 chemistry, 10× Genomics) for the control experiment or a Chromium Single Cell 3' GEM, Library & Gel Bead Kit (V3 chemistry, 10× Genomics) for the treatment experiment according to the manufacturer's instructions. Libraries were sequenced on a NovaSeq 6000 (Illumina) instrument following the 10× Genomics recommendations at the VIB Nucleomics Core facility (VIB, Leuven).

**ScRNA-seq Dataset Analysis.** The raw sequencing data were demultiplexed with the 10× CellRanger (version 3.1.0) software "cellranger mkfastq." The fastq files obtained after demultiplexing were used as the input for "cellranger count," which aligns the reads to the Arabidopsis reference genome (Ensemble TAIR10.40) using STAR and collapses them to unique molecular identifier (UMI) counts. The result is a large digital expression matrix with cell barcodes as rows and gene identities as columns. Initial filtering in CellRanger recovered 13,796 cells for the control (*TMMpro:TMM-GFP*), 9,217 cells for the DMSO treatment, 8,384 cells for the BL treatment, and 8,198 cells for the bikinin treatment (*TMMpro:GFP*) samples, corresponding to 20,842 mean reads and 1,520 median genes, 37,828 mean reads and 2,132 median genes, 38,102 mean reads and 2,656 median genes, and 37,770 mean reads and 2,088 median genes per

cell, respectively. To ensure that only high-quality cells were further analyzed, the filtered data provided by CellRanger were used as input for further filtering steps. All analysis were done in *R* (version > 3.6.0). Data were preprocessed by the scater package (version 1.10.1) following a recommended workflow (51). Outlier cells were defined either as three median absolute deviations (MADs) away from the median value of the UMI numbers or numbers of expressed genes, or as cells containing more than 5% mitochondrial or 10% chloroplastic transcripts. After removal of the outliers, a final number was obtained of 8,180 cells for the control, 5,891 cells for the DMSO treatment, 7,460 cells for the BL treatment, and 6,803 cells for the bikinin treatment samples. Normalization of the raw counts, detection of highly variable genes, discovery of clusters, and creation of UMAP plots were done by means of the Seurat pipeline (version 4.0.3). Cells from the control dataset and the DMSO treatment were integrated into one object with the Harmony package (52) to account for as many different cell types and states as possible. From this object, cells not belonging to the stomatal lineages (e.g., mesophyll and vascular cells) were removed. Differential expression analysis for marker gene identification per subpopulation was based on the nonparametric Wilcoxon rank sum test implemented within the Seurat pipeline. Clusters with the same cell annotation based on gene expression analysis were combined to generate a more comprehensible dataset. Similarly, the DMSO, BL, and bikinin datasets were integrated into one Seurat object with Harmony. This Seurat object was then converted to a SingleCellExperiment object and Slingshot (29) was used to calculate a pseudotime lineage, using "UMAP" as reducedDim, "Pavement" as starting cluster, and "Mature GC" as end cluster. Cells not belonging to the trajectory were removed from the SingleCellExperiment object. The generalized additive models were calculated with the fitGAM command from the tradeSeq package (30) with the different samples as conditions and with six knots, which were determined by the evaluateK function. Expression patterns behaving differently between the treatments were determined with the conditionTest function of tradeSeq and visualized with the plotSmoothers function. To determine whether the cluster "unknown" is induced by protoplasting process, a list of protoplasting-induced genes (53) was used.

**BES1 Dephosphorylation Assay and Quantification.** Arabidopsis seedlings of Col-0, 35Spro:*gPOLAR/Col-0*, or 35Spro:*gPL1/Col-0* were germinated and grown on ½MS agar plates for 5 d and then transferred to liquid ½MS for 2 h and supplemented with 100 nM BL or 50 µM bikinin for 1 h. After treatment, seedlings were harvested and frozen in liquid nitrogen. For the BES1 dephosphorylation analysis, total proteins were extracted with buffer containing 25 mM Tris-HCl, pH 7.5, 150 mM NaCl, 1% (w/v) sodium dodecyl sulfate (SDS), 10 mM dithiothreitol (DTT), and EDTA-free protease inhibitor mixture complete (Roche Diagnostics). For blocking and antibody dilutions, 5% (w/v) skim milk powder in Tris-buffered saline containing 0.2% (v/v) TWEEN20 was used. Proteins were resolved by 10% SDS-polyacrylamide gel electrophoresis (PAGE) and detected by western blot with polyclonal anti-BES1(3) and anti-tubulin (Sigma-Aldrich). Dephosphorylated BES1, phosphorylated BES1, and tubulin proteins were quantified based on the signal intensity with ImageJ (<https://imagej.nih.gov/ij/>). Full blots are shown in *SI Appendix*, Fig. S11.

**qRT-PCR.** RNA was extracted from 100 mg of seedlings at 3 dpg by means of the RNeasy mini kit (Qiagen) according to the manufacturer's instructions. cDNA was generated with the qScript cDNA SuperMix (Quantabio). For the qRT-PCR, a LightCycler® 480 machine (Roche Diagnostics) was used with SYBR green I qPCR master mix (Roche Diagnostics). For the validation of gene expression identified in the scRNA-seq analysis, RNA was extracted from 20,000 to 50,000 GFP-positive cells sorted from the protoplasts of Arabidopsis cotyledons expressing *TMMpro:GUS-GFP*. Cotyledons were harvested at 5 dpg after treatment with 1 µM BL, 50 µM bikinin, or 0.1% (v/v) DMSO for 2 h. Primers are listed in *SI Appendix*, Table S2.

**Quantitative Analysis of Epidermal Phenotypes.** For epidermal cell analysis of developing cotyledons of Arabidopsis seedlings at 3 dpg, cotyledons were stained by propidium iodide (50 µg/mL) and imaged with a SP8 confocal microscope (Leica). Epidermal cell surface areas in a 0.125-mm<sup>2</sup> region from the central part of a cotyledon were measured in ImageJ with a free-hand selection tool. Cell density and stomatal index were calculated as number of cells/mm<sup>2</sup> and number of stomata/total number of cells × 100, respectively.

**Microscopy, Image Acquisition, and Image Analysis.** The abaxial side of cotyledons of *Arabidopsis* seedlings at 3 dpg or infiltrated *N. benthamiana* leaves were analyzed with a SP8 confocal microscope (Leica). The images were taken at 405 nm, 488 nm, and 559 nm laser excitation and 425 to 460 nm, 500 to 530 nm, and 570 to 670 nm long-pass emission for TagBFP2, eGFP, and mCherry/propidium iodide/FM 4-64, respectively. The gating system was applied for autofluorescence removal. The z stack images were taken with an interval of 4  $\mu$ m.

*N*-(3-triethylammoniumpropyl)-4-(6-(4-(diethylamino) phenyl) hexatrienyl) pyridinium dibromide (FM 4-64; 50  $\mu$ M) (Invitrogen) and propidium iodide (PI; 50  $\mu$ g/mL) (Sigma-Aldrich) were used for staining the PM in cotyledon epidermis. Dihydrochloride (DAPI; 0.5  $\mu$ g/ $\mu$ L) (Invitrogen) was used for nuclear staining. For time-lapse imaging, cotyledons of *Arabidopsis* seedlings at 2 dpg were mounted in a chamber filled with 1/2MS agar. The z stack images were captured at 40-min intervals during the time indicated. The movies were made at the speed of three frames per second (f.p.s.). For quantification of the nucleus BES1-GFP intensity, the Fiji image analysis software (<http://fiji.sc>) was used. For measurement of fluorescence intensity changes upon BL or bikinin treatment, the abaxial side of cotyledons at 5 dpg was analyzed. All the fluorescent nuclei were outlined with the “Analyze particles” function of the Fiji software. The mean gray value of the each selected area was then measured.

**Co-IP Assay.** The plant materials were ground into powder with liquid nitrogen and resuspended in extraction buffer [50 mM Tris-HCl, pH 7.5, 50 mM NaCl, 300 mM sucrose, 1% (v/v) Triton X-100, 1× protease inhibitor, and 0.2 mM phenylmethylsulfonyl fluoride]. After centrifugation at 15,000g for 10 min, the supernatants were incubated with GFP trap magnetic agarose for 1 h. Beads were washed four times with extraction buffer containing 0.2% (v/v) Triton X-100 and eluted with 2× SDS sample buffer [24 mM Tris-HCl, pH 6.8, 10% (v/v) glycerol, 0.8% (w/v) SDS, and 2% (v/v) 2-mercaptoethanol].

**Purification of Bacterially Produced Proteins.** The recombinant plasmids of *pDEST-HIS-MBP-POLAR*, *pDEST-HIS-MBP-PL1*, *pDEST-HIS-MBP-GFP*, and *pET-SUMO-SH-BIN2* were transformed into *E. coli* BL21 Rosetta (DE3) cells. MBP-HIS-POLAR, MBP-HIS-PL1, and MBP-HIS-GFP proteins were purified with amylose resin (NEB) and SUMO-HIS-BIN2 protein was purified with Ni-NTA Agarose (Qiagen). Full blots are shown in *SI Appendix*, Fig. S11.

**In Vitro Kinase Assay.** MBP bead-bound MBP-HIS-GFP, MBP-HIS-POLAR, and MBP-HIS-PL1 proteins were incubated with SUMO-HIS-BIN2 in kinase assay buffer (50 mM Tris-HCl, pH 7.5, 100 mM NaCl, 10 mM MgCl<sub>2</sub>, and 1 mM DTT), 100  $\mu$ M cold ATP, and 5  $\mu$ Ci ( $\gamma$ -<sup>32</sup>P)ATP for 2 h at 30 °C. After the reaction, each supernatant fraction of SUMO-HIS-BIN2 was collected and separated by SDS-PAGE. Full blots are shown in *SI Appendix*, Fig. S11.

**Nuclear and Cytoplasmic Fractionation.** Subcellular fractionation was carried out as described previously (54). *Arabidopsis* seedlings were ground in liquid nitrogen and extracted with lysis buffer [20 mM HEPES, pH 7.5, 40 mM KCl, 10% (v/v) glycerol, 1 mM EDTA, 10 mM MgCl<sub>2</sub>, and 1% (v/v) Triton X-100]. Each

extract was filtered and centrifuged at 5000g for 2 min. The supernatants were collected as cytoplasmic fractions, and the pellets were washed several times with the buffer. Clear nuclear pellets were resuspended with the same volume as that of the cytosolic fraction. Nuclear and cytosolic fractions were mixed with SDS sample buffer and separated by SDS-PAGE. Anti-H3 and anti-PEPC were applied to detect nuclear and cytoplasmic marker, respectively. Full blots are shown in *SI Appendix*, Fig. S11.

**Statistical Analysis.** All statistical analysis were performed in GraphPad Prism 9 software except for the box plots. All the box plots were generated by BoxPlotR (55) and P values were calculated by single-factor ANOVA. Details of statistical analysis are provided in the figure legends.

**Data, Materials, and Software Availability.** The scRNA-seq datasets are available at the NCBI Gene Expression Omnibus repository under accession number GSE193451 (56). All study data are included in the article and/or [supporting information](#).

**ACKNOWLEDGMENTS.** We thank Y. Yin (Iowa State University) for the BES1 antibody, A. Vatén (University of Helsinki), X. Wang (Henan University), C. Fenoll (University of Castilla-La Mancha), T. Kakimoto (Osaka University), D. Bergmann (Stanford University), K. Torri (University of Texas at Austin), L. De Veylder (VIB-UGent), Z. Wang (Carnegie Institute), A. Molina (CBGP, UPM-INIA), and M. Mena (The University of Castilla-La Mancha) for sharing published materials, N. Vukašinović for useful discussion and Martine De Cock for help in preparing the manuscript. The CYCD7;1pro:GFP-GUS line was a kind gift from L. De Veylder (VIB-UGent). We are thankful to the VIB Single Cell Core, VIB Flow Core Ghent and VIB Nucleomics for support and access to the instrument park (vib.be/core-facilities). This work is supported by Research Foundation-Flanders (project G003720N to E.R. and a postdoctoral fellowship 1222221N to E.-J.K.), Chinese Scholarship Council (predoctoral fellowships to C.Z. and B.G. and a visiting scientist fellowship to K.W.), Belgian Science Policy (postdoctoral fellowship M.T. and K.W.), Ghent University “Bijzondere Onderzoeksfonds” (BOF/CHN/010 to C.Z. and BOF18/DPO/151 to J.R.W.), and European Research Council (ERC Starting Grant TORPEDO, no. 714055 to B.D.R.).

Author affiliations: <sup>a</sup>Department of Plant Biotechnology and Bioinformatics, Ghent University, Ghent 9052, Belgium; <sup>b</sup>Center for Plant Systems Biology, VIB, Ghent 9052, Belgium; <sup>c</sup>College of Life Sciences, Wuhan University, Wuhan 430072, China; <sup>d</sup>VIB Single Cell Core, VIB, Ghent 9052, Belgium; <sup>e</sup>Department of Applied Mathematics, Computer Science and Statistics, Ghent University, Ghent 9000, Belgium; and <sup>f</sup>Data Mining and Modeling for Biomedicine, Center for Inflammation Research, VIB, Ghent 9052, Belgium

Author contributions: E.-J.K., C.Z., B.G., A.H., K.W., Y.Z., B.D.R., and E.R. designed research; E.-J.K., C.Z., B.G., A.H., J.R.W., M.T., C.S.-V., and I.V. performed research; Y.S. and B.D.R. contributed new reagents/analytic tools; E.-J.K., C.Z., B.G., T.E., and N.V. analyzed data; and E.-J.K., C.Z., B.G., T.E., B.D.R., and E.R. wrote the manuscript.

Reviewers: A.C.-D., Centre for Research in Agricultural Genomics, Barcelona; S.A.C., University of Sheffield; and I.E., Hebrew University of Jerusalem.

The authors declare no competing interest.

1. T. M. Nolan, N. Vukašinović, D. Liu, E. Russinova, Y. Yin, Brassinosteroids: Multidimensional regulators of plant growth, development, and stress responses. *Plant Cell* **32**, 295–318 (2020).
2. Z.-Y. Wang *et al.*, Nuclear-localized BZR1 mediates brassinosteroid-induced growth and feedback suppression of brassinosteroid biosynthesis. *Dev. Cell* **2**, 505–513 (2002).
3. Y. Yin *et al.*, BES1 accumulates in the nucleus in response to brassinosteroids to regulate gene expression and promote stem elongation. *Cell* **109**, 181–191 (2002).
4. T.-W. Kim *et al.*, Brassinosteroid signal transduction from cell-surface receptor kinases to nuclear transcription factors. *Nat. Cell Biol.* **11**, 1254–1260 (2009).
5. J.-Y. Zhu *et al.*, The F-box protein KIB1 mediates brassinosteroid-induced inactivation and degradation of GSK3-like kinases in *Arabidopsis*. *Mol. Cell* **66**, 648–657.e4 (2017).
6. X.-M. Luo *et al.*, Integration of light- and brassinosteroid-signaling pathways by a GATA transcription factor in *Arabidopsis*. *Dev. Cell* **19**, 872–883 (2010).
7. X. Yu *et al.*, A brassinosteroid transcriptional network revealed by genome-wide identification of BES1 target genes in *Arabidopsis thaliana*. *Plant J.* **65**, 634–646 (2011).
8. G. E. Gudeblat *et al.*, SPEECHLESS integrates brassinosteroid and stomata signalling pathways. *Nat. Cell Biol.* **14**, 548–554 (2012).
9. T.-W. Kim, M. Michniewicz, D. C. Bergmann, Z.-Y. Wang, Brassinosteroid regulates stomatal development by GSK3-mediated inhibition of a MAPK pathway. *Nature* **482**, 419–422 (2012).
10. M. Khan *et al.*, Brassinosteroid-regulated GSK3/Shaggy-like kinases phosphorylate mitogen-activated protein (MAP) kinase kinases, which control stomata development in *Arabidopsis thaliana*. *J. Biol. Chem.* **288**, 7519–7527 (2013).
11. A. Houbaert *et al.*, POLAR-guided signalling complex assembly and localization drive asymmetric cell division. *Nature* **563**, 574–578 (2018).
12. L. J. Pillitteri, K. U. Torii, Mechanisms of stomatal development. *Annu. Rev. Plant Biol.* **63**, 591–614 (2012).
13. A. Hermann, K. U. Torii, Shouting out loud: Signaling modules in the regulation of stomatal development. *Plant Physiol.* **185**, 765–780 (2011).
14. J. Dong, C. A. MacAlister, D. C. Bergmann, BASL controls asymmetric cell division in *Arabidopsis*. *Cell* **137**, 1320–1330 (2009).
15. O. S. Lau *et al.*, Direct roles of SPEECHLESS in the specification of stomatal self-renewing cells. *Science* **345**, 1605–1609 (2014).
16. L. J. Pillitteri, K. M. Peterson, R. J. Horst, K. U. Torii, Molecular profiling of stomatal meristemoids reveals new component of asymmetric cell division and commonalities among stem cell populations in *Arabidopsis*. *Plant Cell* **23**, 3260–3275 (2011).
17. M. H. Rowe, J. Dong, A. K. Weimer, D. C. Bergmann, A plant-specific polarity module establishes cell fate asymmetry in the *Arabidopsis* stomatal lineage. *BioRxiv* [Preprint] (2019). <https://doi.org/10.1101/614636> (Accessed 19 April 2019).
18. X. Guo, C. H. Park, Z. Y. Wang, B. E. Nickels, J. Dong, A spatiotemporal molecular switch governs plant asymmetric cell division. *Nat. Plants* **7**, 667–680 (2021).
19. B. De Rybel *et al.*, Chemical inhibition of a subset of *Arabidopsis thaliana* GSK3-like kinases activates brassinosteroid signaling. *Chem. Biol.* **16**, 594–604 (2009).
20. A. de Marcos *et al.*, A mutation in the bHLH domain of the SPCH transcription factor uncovers a BR-dependent mechanism for stomatal development. *Plant Physiol.* **174**, 823–842 (2017).
21. N. Vukašinović *et al.*, Local brassinosteroid biosynthesis enables optimal root growth. *Nat. Plants* **7**, 619–632 (2021).

22. J. A. Nadeau, F. D. Sack, Control of stomatal distribution on the *Arabidopsis* leaf surface. *Science* **296**, 1697–1700 (2002).
23. E. Becht *et al.*, Dimensionality reduction for visualizing single-cell data using UMAP. *Nat. Biotechnol.* **37**, 38–44 (2019). 10.1038/nbt.4314.
24. C. B. Lopez-Anido *et al.*, Single-cell resolution of lineage trajectories in the *Arabidopsis* stomatal lineage and developing leaf. *Dev. Cell* **56**, 1043–1055 (2021).
25. J. Adrian *et al.*, Transcriptome dynamics of the stomatal lineage: Birth, amplification, and termination of a self-renewing population. *Dev. Cell* **33**, 107–118 (2015).
26. Z. Liu *et al.*, Global dynamic molecular profiling of stomatal lineage cell development by single-cell RNA sequencing. *Mol. Plant* **13**, 1178–1193 (2020).
27. C.-M. K. Ho, M. Bringmann, Y. Oshima, N. Mitsuda, D. C. Bergmann, Transcriptional profiling reveals signatures of latent developmental potential in *Arabidopsis* stomatal lineage ground cells. *Proc. Natl. Acad. Sci. U.S.A.* **118**, e2021682118 (2021).
28. S. Vanneste *et al.*, Developmental regulation of CYCA2s contributes to tissue-specific proliferation in *Arabidopsis*. *EMBO J.* **30**, 3430–3441 (2011).
29. K. Street *et al.*, Slingshot: Cell lineage and pseudotime inference for single-cell transcriptomics. *BMC Genomics* **19**, 477 (2018).
30. K. Van den Berghe *et al.*, Trajectory-based differential expression analysis for single-cell sequencing data. *Nat. Commun.* **11**, 1201 (2020).
31. S.-K. Han *et al.*, Deceleration of the cell cycle underpins a switch from proliferative to terminal divisions in plant stomatal lineage. *Dev. Cell* **57**, 569–582 (2022).
32. M. Hashimoto *et al.*, *Arabidopsis* HT1 kinase controls stomatal movements in response to CO<sub>2</sub>. *Nat. Cell Biol.* **8**, 391–397 (2006).
33. G. Pilot *et al.*, Guard cell inward K<sup>+</sup> channel activity in *Arabidopsis* involves expression of the twin channel subunits KAT1 and KAT2. *J. Biol. Chem.* **276**, 3215–3221 (2001).
34. P. Peng, Z. Yan, Y. Zhu, J. Li, Regulation of the *Arabidopsis* GSK3-like kinase BRASSINOSTEROID-INSENSITIVE 2 through proteasome-mediated protein degradation. *Mol. Plant* **1**, 338–346 (2008).
35. J. Jiang, C. Zhang, X. Wang, A recently evolved isoform of the transcription factor BES1 promotes brassinosteroid signaling and development in *Arabidopsis thaliana*. *Plant Cell* **27**, 361–374 (2015).
36. K. A. Davies, D. C. Bergmann, Functional specialization of stomatal bHLHs through modification of DNA-binding and phosphoregulation potential. *Proc. Natl. Acad. Sci. U.S.A.* **111**, 15585–15590 (2014).
37. S. D. Clouse, Brassinosteroids. *Arabidopsis Book* **9**, e0151 (2011).
38. W. Chen *et al.*, BES1 is activated by EMS1-TPD1-SERK1/2-mediated signaling to control tapetum development in *Arabidopsis thaliana*. *Nat. Commun.* **10**, 4164 (2019).
39. M. Wang, K. Yang, J. Le, Organ-specific effects of brassinosteroids on stomatal production coordinate with the action of TOO MANY MOUTHS. *J. Integr. Plant Biol.* **57**, 247–255 (2015).
40. A. K. Weimer *et al.*, Lineage- and stage-specific expressed *CYCD7;1* coordinates the single symmetric division that creates stomatal guard cells. *Development* **145**, dev160671 (2018).
41. P. Anne *et al.*, OCTOPUS negatively regulates BIN2 to control phloem differentiation in *Arabidopsis thaliana*. *Curr. Biol.* **25**, 2584–2590 (2015).
42. C. Zhang *et al.*, ROPGAP-dependent interaction between brassinosteroid and ROP2-GTPase signaling controls pavement cell shape in *Arabidopsis*. *Curr. Biol.* **32**, 518–531 e516 (2022).
43. K. Hara, R. Kajita, K. U. Torii, D. C. Bergmann, T. Kakimoto, The secretory peptide gene EPF1 enforces the stomatal one-cell-spacing rule. *Genes Dev.* **21**, 1720–1725 (2007).
44. L. J. Pillitteri, D. B. Sloan, N. L. Bogenschutz, K. U. Torii, Termination of asymmetric cell division and differentiation of stomata. *Nature* **445**, 501–505 (2007).
45. C. A. MacAlister, K. Ohashi-Ito, D. C. Bergmann, Transcription factor control of asymmetric cell divisions that establish the stomatal lineage. *Nature* **445**, 537–540 (2007).
46. K. Ohashi-Ito, D. C. Bergmann, *Arabidopsis* FAMA controls the final proliferation/differentiation switch during stomatal development. *Plant Cell* **18**, 2493–2505 (2006).
47. D. Yi *et al.*, The *Arabidopsis* SIAMESE-RELATED cyclin-dependent kinase inhibitors SMR5 and SMR7 regulate the DNA damage checkpoint in response to reactive oxygen species. *Plant Cell* **26**, 296–309 (2014).
48. A. Lampropoulos *et al.*, GreenGate—A novel, versatile, and efficient cloning system for plant transgenesis. *PLoS One* **8**, e83043 (2013).
49. W. Decaecker *et al.*, CRISPR-TSKO: A technique for efficient mutagenesis in specific cell types, tissues, or organs in *Arabidopsis*. *Plant Cell* **31**, 2868–2887 (2019).
50. B. O. R. Bargmann, K. D. Birnbaum, Fluorescence activated cell sorting of plant protoplasts. *J. Vis. Exp.*, 1673 (2010).
51. A. T. L. Lun, K. Bach, J. C. Marioni, Pooling across cells to normalize single-cell RNA sequencing data with many zero counts. *Genome Biol.* **17**, 75 (2016).
52. I. Korsunsky *et al.*, Fast, sensitive and accurate integration of single-cell data with Harmony. *Nat. Methods* **16**, 1289–1296 (2019).
53. K. Birnbaum *et al.*, A gene expression map of the *Arabidopsis* root. *Science* **302**, 1956–1960 (2003).
54. Y. T. Cheng *et al.*, Nuclear pore complex component MOS7/Nup88 is required for innate immunity and nuclear accumulation of defense regulators in *Arabidopsis*. *Plant Cell* **21**, 2503–2516 (2009).
55. M. Spitzer, J. Wildenhain, J. Rappaport, M. Tyers, BoxPlotR: A web tool for generation of box plots. *Nat. Methods* **11**, 121–122 (2014).
56. E.-J. Kim *et al.*, Cell type-specific attenuation of brassinosteroid signaling precedes stomatal asymmetric cell division. *Gene Expression Omnibus*. <https://www.ncbi.nlm.nih.gov/geo/query/acc.cgi?acc=GSE193451>. Deposited 11 January 2022.